

Growth of half-metallic CrO₂ nanostructures for superconducting spintronic applications

A. Singh¹, C. Jansen¹, K. Lahabi¹, & J. Aarts¹

¹*Kamerlingh Onnes-Huygens Laboratory, Leiden University,
P.O. Box 9504, 2300 RA Leiden, The Netherlands.*

(Dated: October 1, 2018)

Superconductor-ferromagnet (S-F) hybrids based on half-metallic ferromagnets, such as CrO₂, are excellent candidates for superconducting spintronic applications. This is primarily due to their fully spin polarized nature, which produces significantly enhanced long-range triplet proximity effects. However, reliable production of CrO₂-based Josephson junctions (JJs) is challenging, mainly because of the difficulty to control the transparency of the S/F interface. We have grown CrO₂ nanowires by chemical vapor deposition on TiO₂ substrates combined with selective area growth in trenches defined with amorphous SiO_x. This allows us to create lateral JJs, with the nanowire as the weak link. We show that the nature of the growth is highly anisotropic, and that the morphology of the CrO₂ nanostructures changes systematically during the growth process, depending on the width of the trench. The detailed growth study enables us to synthesise multifaceted and highly homogeneous CrO₂ wires. These are utilized to fabricate JJs with high S/F interface transparency, leading to large supercurrents. The well-defined geometry of the device allows us to reliably estimate an exceptionally high critical current density $J_c = 10^9 \text{ Am}^{-2}$ over a distance of 600 nm.

Superconductor/Ferromagnet (S/F) hybrids have attracted great interest due their potential application in spintronic devices to minimize the dissipation/Joule heating, which is the biggest challenge for current-driven processes at the nanoscale [1–3]. The novelty of such hybrids lies in the generation of spin polarized triplet Cooper pairs in the ferromagnet [4–6]. They are generated by subjecting singlet Cooper pairs at the S/F interface to spin mixing and rotation [7], which is usually achieved by introducing another thin ferromagnetic layer at the interface [8–11]. Since triplet Cooper pairs are not affected by the exchange field of the ferromagnet, they can survive over considerably long distances, thereby giving rise to spin-polarized supercurrents. Fully spin polarized CrO₂ is an ideal ferromagnet for such applications. The spatial extent of induced triplet correlations in CrO₂ is of the order of a micron [12, 13], while it is limited to few tens of nm for standard ferromagnets (Co, Ni, Fe). Furthermore, the efficiency of the triplet generation is significantly enhanced, as demonstrated in recent experiments in a spin valve geometry [14, 15]. Though large supercurrents have been observed in CrO₂ films [16], a serious bottleneck for further studies and applications of such Josephson junctions (JJs) has been the poorly controlled interface transparency, together with ill-defined current paths in the full film. Etching wire structures out of films proved no solution since the resist mask and the etch step are detrimental to the surface and bring extra disorder in the material. To address this issue, we have made a detailed investigation into the growth of CrO₂ nanowires by selective area chemical vapor deposition (CVD).

A salient feature of the CVD growth of CrO₂ is that it is only known to grow epitaxially on TiO₂ or sapphire substrates. This is an advantage for selective area growth (SAG), whereby a patterned SiO_x mask can be used to

define the geometry of the CrO₂ nanostructures. Previous reports on SAG of CrO₂ focussed on the morphology of thick CrO₂ structures but did not give insight into the nucleation and growth kinetics at the early stage of growth [17, 18]. Here, we demonstrate the effect of mask confinement, lattice mismatch anisotropy, and trench aspect ratio on the magnetic and structural morphology of CrO₂ nanostructures at different stages of growth, covering a wide range of film thicknesses. A better understanding of SAG allows us to create high quality uniform CrO₂ nanowires with well-defined facets resulting in transparent interfaces. In addition, we show that the magnetization state of the nanowire can be controlled by exploiting its shape anisotropy. This robust control over the magnetization and transparency enables us to reproducibly fabricate CrO₂-based JJs with large critical current densities. More generally, we have developed a device platform which will allow for a large variety of different wire, contact and magnetic domain geometries.

Selective Area Growth We start with a rutile (100) TiO₂ substrate which has a tetragonal surface net ($b = 0.459 \text{ nm}$, $c = 0.296 \text{ nm}$), on which CrO₂ ($b = 0.442 \text{ nm}$, $c = 0.292 \text{ nm}$) can be grown isostructurally. The lattice mismatch is anisotropic, being -1.4 % along the b -axis and -3.8 % along the c -axis, respectively. This leads to anisotropic growth rates, which is important for nanowire growth. Substrates were cleaned with organic solvents (Acetone/IPA) followed by HF treatment, on which a 25 nm SiO_x thin film was sputter-deposited. Using e-beam resist and lithography, openings of different sizes and shapes were created in the resist along different crystallographic directions. SiO_x was selectively removed from the openings using RIE etching with a CF₄- and an O₂-plasma. The etch time of SiO_x is critical because underetching results in only partial removal

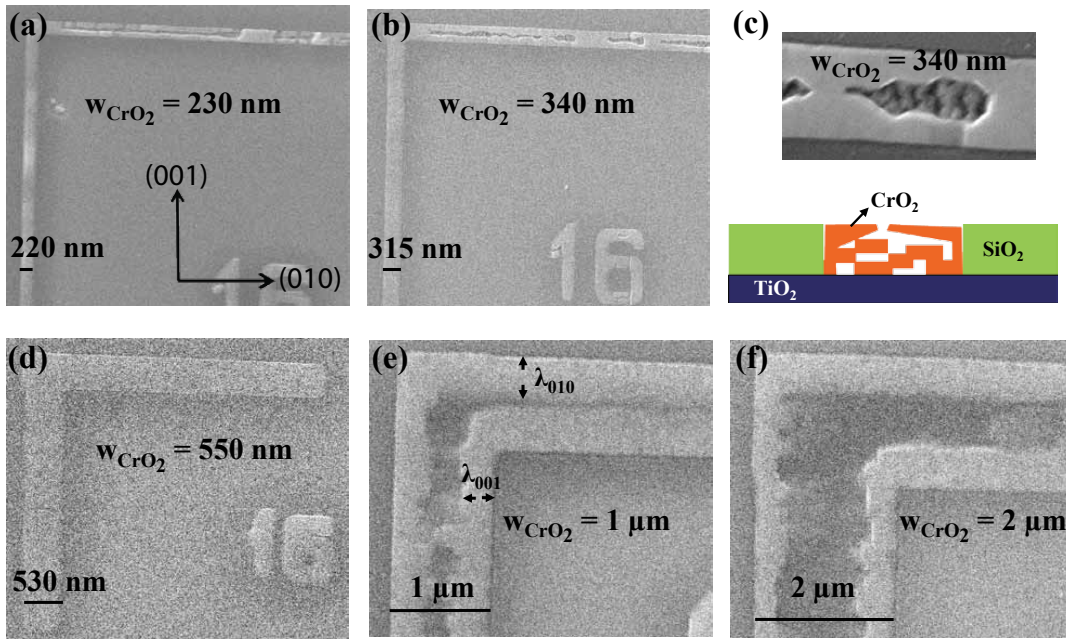


Figure 1: Scanning electron micrographs of L-shaped nanowires along the indicated directions, grown for 20 minutes, with trench widths (a) 230 nm, (b) 340 nm, (c) 340 nm, a close-up. The lower half schematically illustrates the growth mode for trench widths (d) 550 nm, (e) 1 μm , and (f) 2 μm . The measured width of the CrO_2 bars is shown, and found equal to the trench width. In (d) λ is a measure for the surface diffusion length.

of SiO_x while overetching damages the underlying TiO_2 substrate, which affects the film quality adversely. Next, CrO_2 was grown selectively in the SiO_x trenches (trench depth 25 nm, trench width w_{trench}) by CVD in a two-zone furnace where the substrate temperature was kept at 395°C while the precursor CrO_3 was heated to 260°C in the presence of a flow of 100 sccm O_2 carrier gas. By monitoring the growth times (t_g), samples with varying thicknesses were prepared. Each sample consists of CrO_2 structures with different sizes, shapes, aspect ratios and orientations. Scanning electron microscopy (SEM), Atomic force microscopy (AFM), and Magnetic force microscopy (MFM) were used to examine the structural and magnetic morphology of the CrO_2 nanostructures.

In-trench growth Fig. 1a-e show the SEM images of L-shaped nanowires, grown for 20 minutes, with w_{trench} varying from 230 nm to 2 μm . The time is chosen such that it fills the 25 nm deep trench. For the discussion, the width range is divided into two regimes, Regime I : $w_{\text{trench}} \leq 2\lambda$, and Regime II: $w_{\text{trench}} \geq 2\lambda$, where λ is a characteristic length bearing resemblance to a surface diffusion length, which is anisotropic due to the anisotropic lattice mismatch. For free films, growth results in the formation of rectangular CrO_2 grains with their long axis along [001] and with an average size of $\sim 300 \text{ nm} \times 100 \text{ nm}$, which sets the scale for λ . In the strongly confined structures shown in Fig.1a-b, nucleation and growth is clearly anisotropic, with homogeneous wires forming along [001] and more inhomogeneous growth along [010]. This can

be understood from the better lattice match along [001] which also is the unconfined direction. Individual grains grow faster and coalesce to form a continuous and homogeneous wire. Along [010] the wires grow in a peculiar fashion, namely *from the sides* rather than from the bottom. Fig. 1c shows a close-up of the 340 nm trench where a smooth surface is seen at the sides, and a hole in the middle where, at the bottom, growth has also started. Apparently, CrO_2 islands nucleate preferably at the $\text{SiO}_x/\text{TiO}_2$ interface and grow laterally inward but also vertically upward. This dynamically inhibits the supply of the reactants towards the bottom of the trench, but it does allow inward lateral overgrowth starting higher up the wall. The result is a disordered structure with voids. This so-called nanopendeo-epitaxy overgrowth (nPEO) is known from semiconductor growth, in particular for GaN, in the fabrication of nanoairbridges and suspended structures of GaN with superior quality [19–21].

At $w_{\text{trench}} = 550 \text{ nm}$ (Fig.1d) Regime II starts and the growth changes to a homogeneous filling of the trench [22]. Islands nucleate along the walls and "quantum fortress"-like structures are formed irrespective of the orientation of trenches [23]. Increasing w_{trench} to 1 μm and 2 μm (Fig.1e,f) the filling becomes inhomogeneous again, with the middle of the trench empty but now because the growth fronts propagating from the walls do not reach the middle. We assume that the size of the CrO_2 strip along the walls is determined by λ and we

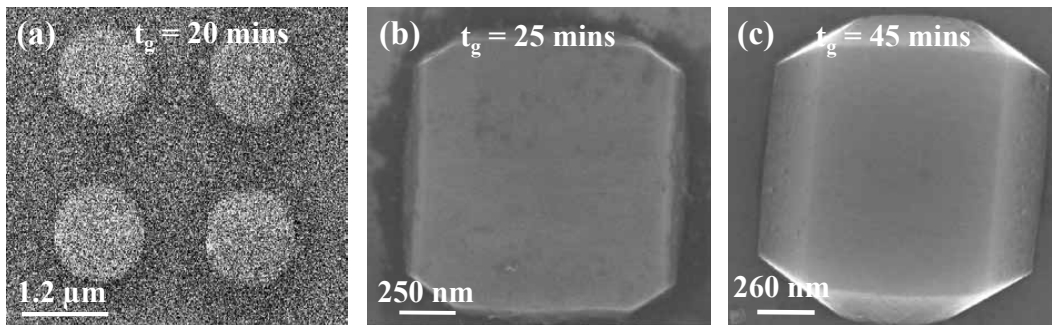


Figure 2: Scanning electron micrographs of CrO₂ structures, grown in circular SiO₂ trenches, for (a) 20 minutes (filling the disk-shaped trench), (b) 25 minutes, and (c) 45 minutes. The latter two are overgrowth structures.

observe $\lambda_{010} \sim 450$ nm and $\lambda_{010} \sim 300$ nm independent of w_{trench} . Note that these results are quite different from earlier reports on SAG of CrO₂, where it was assumed that CrO₂ nucleates and grows uniformly in the narrow trenches away from the SiO_x side walls [18]. Our results present a very different picture, with important new aspects for CrO₂ nanowire growth.

Lateral overgrowth Next we focus on the lateral epitaxial overgrowth (LEO) above the SiO_x mask at higher t_g . Fig. 2a-c shows the evolution of the structural morphology of CrO₂, grown in circular trenches, for different t_g . For $t_g = 20$ minutes, no overgrowth yet occurs, resulting in the formation of CrO₂ discs. With further increase in t_g (25 minutes), CrO₂ starts to overgrow laterally on SiO_x. Important to realize is that there is no epitaxial relation with the amorphous SiO_x, so this is sideways growth starting from the structure coming out of the trench. The development of (011) facets can be observed, assumedly to minimize the total surface energy, although the facets formed at this stage are rough with step edges. For $t_g = 45$ minutes, the CrO₂ islands exhibit fully developed facets with smooth surfaces. This type of facet evolution with growth time has been reported recently for SAG of GaN [22].

In order to isolate the effect of lattice mismatch and size on the issue of CrO₂ overgrowth, we also prepared rectangular 500 nm wide SiO_x trenches oriented between the (010)- ($\theta = 0^\circ$) and (001)-directions ($\theta = 90^\circ$), at intervals of 15° . The structural morphologies were characterized at different stages (thicknesses) of growth. In Fig. 3a schematic of the LEO is outlined and Fig 3b,c show the SEM images of CrO₂ nanowires, with $t_g = 20$ minutes, and 45 minutes, respectively. Clearly, there is no anisotropy in the lateral growth for in the first 20 minutes of growth while it is highly anisotropic for $t_g = 45$ minutes. As shown in Fig. 3c, the nanowires exhibit jagged facets at the intermediate angles which is attributed to the higher growth rate along (001) [17]. The anisotropy of lateral overgrowth with SAG has been reported earlier for thick CrO₂ structures [17, 18]. However,

from our data we can extract additional and quantitative information on the anisotropy in lateral as well as vertical overgrowth over a range of sizes and thicknesses. In Fig. 3d we plot the full width of the nanowire as measured from Fig. 3c. This exhibits a maximum at $\theta = 60^\circ$ and becomes more pronounced with increasing t_g . The direction coincides with the diagonal of the CrO₂ unit cell. In Fig. 3e we plot the lateral overgrowth (defined as the difference between the total width of the CrO₂ nanowire and the trench width) as function of θ for different trench widths up to 500 nm (Regime I). The Figure shows that the lateral overgrowth hardly depends on trench width for the various angles, confirming that it is mainly determined by the thickness and anisotropic strain. Finally, to study the anisotropy in vertical growth, AFM was used to determine the thickness of the nanowires grown for different times up to $t_g = 45$ minutes. Fig. 3f again shows suggests that during the first 20 minutes the CrO₂ growth front just reaches the top of the SiO₂ trench and the thickness is isotropic. For higher growth times the vertical overgrowth becomes anisotropic, now with the minimum along $\theta = 60^\circ$: lateral overgrowth clearly goes at the expense of vertical overgrowth, with the largest effect around 60° from the (010)-direction. This is in contrast with the previous reports on SAG of CrO₂ structures where vertical overgrowth was reported to be isotropic [17].

More formally, the correlation between the vertical and the lateral overgrowth, can be understood from the mass transport mechanism i.e. absorption or desorption of adatoms on different facets of CrO₂ during the CVD growth. The vertical growth depends on the impinging flux on top and on the sides of the growing surface and also on the diffusion flux from the substrate to the top surface [24]. The size dependence of the vertical growth rate is given by the following expression,

$$dH/dt = \gamma_{top} + \gamma_{sw}/D + \gamma_{sub}/D^2, \quad (1)$$

where H is the height, D is the width of the structures, γ_{top} , γ_{sw} , and γ_{sub} are the constants related to surface

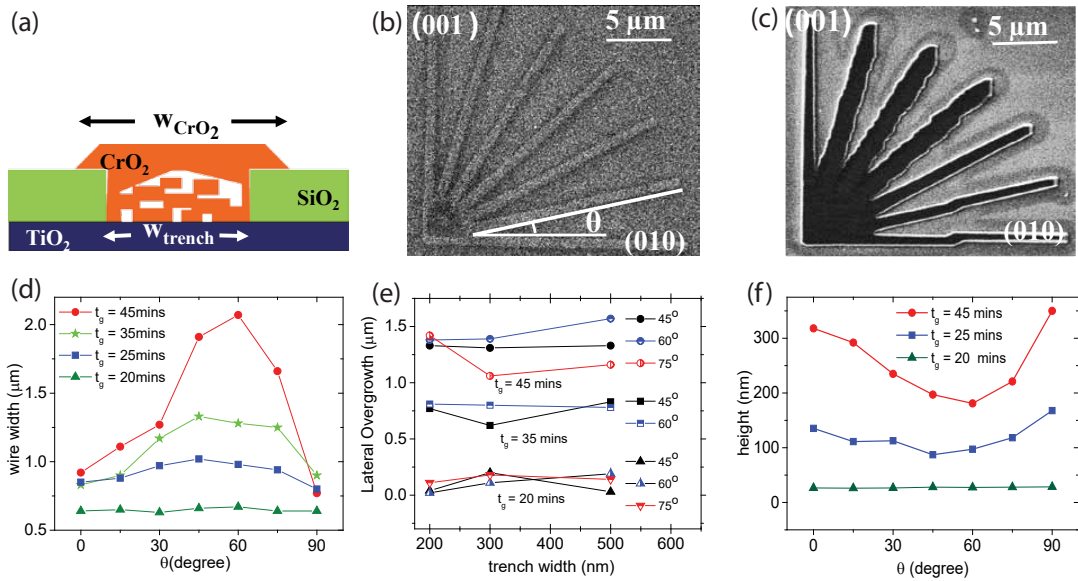


Figure 3: (a) Schematic of lateral epitaxial overgrowth of CrO_2 over SiO_2 for higher growth times. Scanning electron micrographs of CrO_2 nanowires oriented between $\theta = 0^\circ$ and $\theta = 90^\circ$ at the intervals of 15° and grown in 500 nm wide trenches for (b) 20 minutes, and (c) 45 minutes. (d) Angular dependence of width of CrO_2 nanowires (w_{CrO_2}). (e) lateral over growth ($w_{CrO_2} - w_{trench}$) as a function of trench width (w_{trench}) along $\theta = 45^\circ, 60^\circ$, and 75° for different growth times. (f) Angular dependence of height of CrO_2 nanowires, grown in 500 nm wide SiO_x trenches, for different times.

impingement on top and side wall and diffusion from the substrate, respectively. In this simple picture, the maximum lateral overgrowth corresponds to largest D and hence lowest vertical overgrowth. Furthermore, with change in orientation of the wire, γ_{top} remains constant while the contribution from γ_{sw} , and γ_{sub} decreases due to the formation of jagged edges at the intermediate angles. Nonuniform / ragged edges prevent the surface diffusion of adatom on the side walls and also from the substrates, slowing down the vertical overgrowth.

Magnetic domains Next we discuss the magnetic domain structures of our nanowires. Domain behavior has been studied both in early SAG investigations [18] and in etched wires [25, 26] and it is well known that for CrO_2 films on TiO_2 the [001] direction is the magnetic easy axis while the [010] direction is the magnetic hard axis, as a consequence of the strain. Fig.4a shows the magnetic structure of wires of different size along different crystallographic orientations as measured by using magnetic force microscopy (MFM). The wires oriented along [001] are in a single domain state, as seen from the absence of any contrast in MFM image, and in the cross-section shown in the lowest panel of Fig. 4b. When the wire is rotated away from the easy axis, striplike domains start appearing in the wires to minimize the total magnetic energy. This can be seen by dark/bright contrast the MFM micrograph (Fig. 4a) and as oscillations in the magnetic contrast (top and middle panel Fig. 5b). We observe that the domain size is also direction dependent with a minimum along the [001] axis, which is the hard axis. The

wires therefore behave as expected.

Supercurrents As mentioned in the introduction, fully spin-polarized ferromagnetic nanowires are of interest for superspintronics applications, and here we show that we can fabricate Josephson junctions with the CrO_2 nanowire as weak link. First we grow a nanowire along the easy axis [001] in order to have the magnetization along the wire axis. Next we use lift-off and sputtering to deposit rectangularly shaped contacts of $(Cu \text{ or } Ag)(5 \text{ nm})/Ni(1.5 \text{ nm})/MoGe(125 \text{ nm})$ trilayer stacks, with their long axis perpendicular to CrO_2 wire, i.e. along the [010] direction as shown in Fig. 5a. The distance between the contacts is typically 500 nm. The shape anisotropy aligns the magnetization of the Ni layer in the contact stack along the crystal [010] direction, which is very effective in providing maximum non-collinearity at the interface, a key ingredient for triplet generation. In the trilayer stack we used either Cu or Ag to prevent exchange coupling between the CrO_2 and Ni layers. Amorphous MoGe is the superconductor used to induce the proximity effect. Since at the surface CrO_2 inevitably reduces to the antiferromagnetic insulator Cr_2O_3 we clean it in-situ with a brief Ar-etch prior to the trilayer contact deposition. In this report, we present the results obtained on two JJ devices, one with Cu and one with Ag as spacer layer, named J1 and J2, respectively. The other parameters of J1 and J2 are provided in the table below.

Fig.5b shows a plot of resistance R versus temperature (T) for J1 measured in a quasi-4-point geometry, meaning

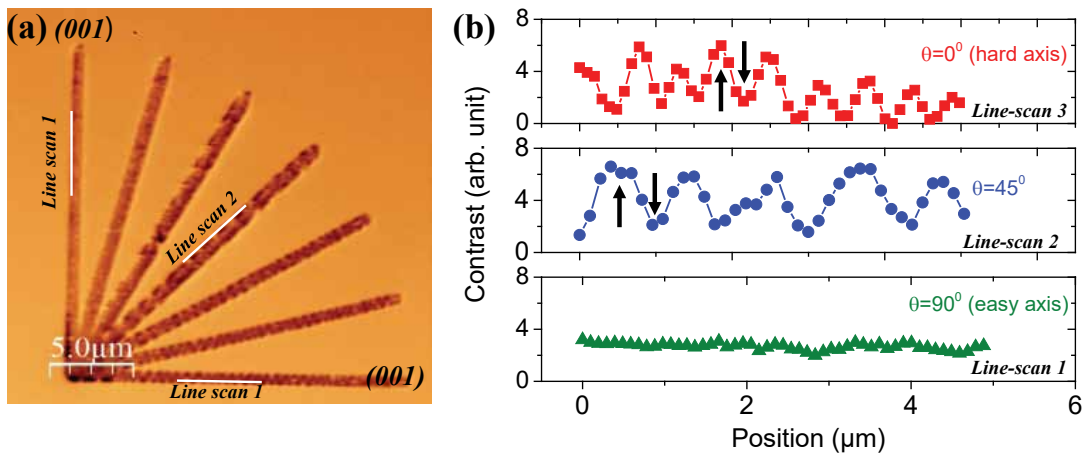


Figure 4: (a) Magnetic force micrograph of CrO₂ nanowires grown in 500 nm wide trench, oriented between $\theta = 0^\circ$ and $\theta = 90^\circ$ at the intervals of 15° . White along the edges of the wires represent the line scan used to determine the phase magnetic phase contrast. (b) Magnetic phase contrast along the edges of the wires for $\theta = 0^\circ$ (upper panel), $\theta = 45^\circ$ (middle panel), and $\theta = 90^\circ$ (lower panel). up and down arrow represent the opposite orientation (180°) domains

Table I: parameters of two Josephson Junction devices based on CrO₂ nanowires. The values for R_N were calculated using a specific resistivity of $6 \mu\Omega\text{cm}$.

Device	width	thickness	junction length	R_N
J1 (Cu)	1 μ	75 nm	400 nm	0.32 Ohm
J2 (Ag)	500 nm	150 nm	600 nm	0.48 Ohm

that the interface resistance is part of the total normal state resistance. R disappears around 6.5 K, but there is a finite resistance tail down to 5 K, where R reaches 0 (c.q. the measurement limit). Below 5 K, supercurrents can be measured. Fig. 5c shows the current-voltage (I-V) characteristics of J1 at different temperatures from which the critical current of the weak link (the proximized CrO₂) can be determined. Interestingly, despite its lower junction length (see Table I), J1 has a lower critical current density than J2, which is probably due to lower interface transparency. Our earlier studies did not use Ag, but the result indicates that the use of Cu might lead to degradation of the interface by the formation of some oxide. Fig. 5d displays the variation of critical current density as a function temperature for J1 and J2, and as expected, I_c increases monotonically with the decrease in temperature. The measured resistance of the device is dominated by the Cu layer in the leads, since the Cu specific resistivity $\rho_{0,Cu}$ of the order of $5 \mu\Omega\text{cm}$ is much smaller than $\rho_{0,MoGe} \approx 200 \mu\Omega\text{cm}$. Taking a length of 70 μm per lead, a width of 2.5 μm and a thickness of 5 nm, we find 560 Ω . The normal resistance of the CrO₂ weak link we estimate using $\rho_{0,CrO_2} \approx 6 \mu\Omega\text{cm}$ (the thin films value for the easy axis) to be 0.32 Ω . This leaves about 20 Ω as the contact resistance. We note in Fig. 5b that the low-temperature R is well below 0.32 Ω , and in Fig. 5c

that the voltage increase above I_c starts with a small steep slope, but then settles to a slope which is close to 0.3 Ω , quite as expected for the CrO₂ weak link. Analyzing the junction behavior a bit further, in the long junction limit I_c is proportional to $T^{3/2} \exp(2\pi k_B T / E_{th})^{-1/2}$ where $E_{th} = \hbar D / L^2$ is the Thouless energy of the junction with diffusion coefficient D and junction length L . Therefore, the slope of the plot of $\ln(I_c) - 3/2 \ln(T)$ vs $T^{1/2}$, shown in the inset, can be used to estimate the Thouless energy E_{Th} which is 11 μV . From this number we can estimate D to be $2.7 \times 10^{-3} \text{ m}^2/\text{s}$, which is close to numbers obtained before. Using a Fermi velocity of $2.2 \times 10^5 \text{ m/s}$ [27] it corresponds to a mean free path of 36 nm which suggests that our JJS are in long (diffusive) junction limit.

Conclusions To conclude, we have made a detailed study of growth kinetics of halfmetallic ferromagnetic CrO₂ nanowires by selective area growth on TiO₂, in 25 nm deep trenches defined by a SiO_x mask. At an early stage of growth ($t_g=20$ minutes), for trench width below 500 nm we find that thin homogeneous wires can be grown along [001], while along [010] the growth is highly disordered, with voids, formed in a fashion called nanopendeo epitaxy. Above a trench width of 500 nm, the trench is lined by CrO₂ strips formed along the edges with nonuniformity at the center. By increasing the growth time, uniform CrO₂ structures are formed due to the lateral overgrowth over SiO_x mask. Wires grown along the magnetic easy axis, which is the [001] direction, were contacted with stacks of Cu/Ni/MoGe and Ag/Ni/MoGe, which allowed us to study triplet supercurrents. This upholds the earlier observation of very high supercurrent densities of order 10^9 A/m^2 at 4.2 K over a distance of 600 nm. CrO₂ wire based Josephson junctions will make it now possible to characterize the in-

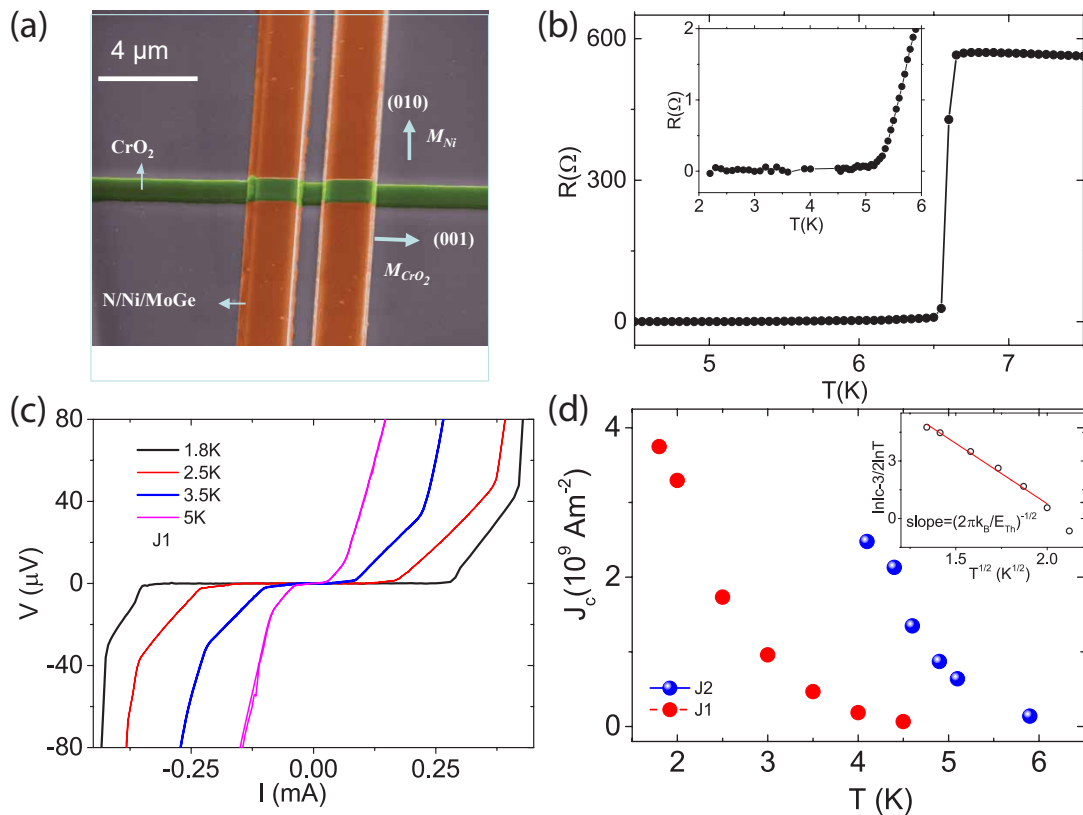


Figure 5: (a). Scanning electron micrograph (false color) of a Josephson Junction on a CrO₂ nanowire (green). The graph also shows crystal and magnetization directions. Orange contacts pads consist of trilayer (Cu or Ag)/Ni/MoGe. (b) Resistance R versus temperature T for junction J1. The inset shows the behavior around zero resistance (c) Current I versus voltage V characteristics of J1 at different temperatures. (d) Critical current density J_c versus T ; the inset shows a linear fit to a plot of $\ln(I_c) - 3/2 \ln(T)$ vs $T^{1/2}$.

interfaces fully, make reliable measurements of the dependence of critical current on junction length, and study the influence of magnetic domains in the supercurrent path.

ACKNOWLEDGEMENTS Technical support from M.B.S. Hesselberth, D. Boltje, and A. F. Beker are gratefully acknowledged. This work is part of the research programme of the Foundation for Fundamental Research on Matter (FOM), which is part of the Netherlands Organisation for Scientific Research (NWO). The work was also supported by the EU COST action MP1201 'NanoSC' and by a grant from the Leiden-Delft Consortium 'NanoFront'.

-
-
- [1] Matthias Eschrig. Spin-polarized supercurrents for spintronics: a review of current progress. *Reports on Progress in Physics*, 78(10):104501, 2015.
 - [2] J. Linder and J. W. A. Robinson. Superconducting spintronics. *Nature Physics*, 11:307, 2015.
 - [3] N. G. Pugach and A. I. Buzdin. *Applied Physics Letters*, 2012.
 - [4] FS Bergeret, AF Volkov, and KB Efetov. Long-range proximity effects in superconductor-ferromagnet structures. *PHYSICAL REVIEW LETTERS*, 86(18):4096–4099, APR 30 2001.
 - [5] M. Eschrig, J. Kopu, J. C. Cuevas, and Gerd Schön. Theory of half-metal/superconductor heterostructures. *Phys. Rev. Lett.*, 90:137003, Apr 2003.
 - [6] M. Houzet and A. I. Buzdin. Long range triplet Josephson effect through a ferromagnetic trilayer. *PHYSICAL REVIEW B*, 76(6), AUG 2007.
 - [7] M. Eschrig and T. Lofwander. Triplet supercurrents in clean and disordered half-metallic ferromagnets. *Nat*

- Phys*, 4:138, 2008.
- [8] Trupti S. Khaire, Mazin A. Khasawneh, W. P. Pratt, Jr., and Norman O. Birge. Observation of Spin-Triplet Superconductivity in Co-Based Josephson Junctions. *PHYSICAL REVIEW LETTERS*, 104(13), APR 2 2010.
- [9] E. C. Gingrich, P. Quarterman, Yixing Wang, R. Loloee, W. P. Pratt, Jr., and Norman O. Birge. Spin-triplet supercurrent in Co/Ni multilayer Josephson junctions with perpendicular anisotropy. *PHYSICAL REVIEW B*, 86(22), DEC 12 2012.
- [10] J. W. A. Robinson, J. D. S. Witt, and M. G. Blamire. Controlled injection of spin-triplet supercurrents into a strong ferromagnet. *Science*, 329(5987):59–61, 2010.
- [11] N. Banerjee, J.W.A. Robinson, and M. G. Blamire. Reversible control of spin-polarized supercurrents in ferromagnetic josephson junctions. *Nat Commun*, 5:4771, 2014.
- [12] RS Keizer, STB Goennenwein, TM Klapwijk, GX Miao, G Xiao, and A Gupta. A spin triplet supercurrent through the half-metallic ferromagnet CrO₂. *NATURE*, 439(7078):825–827, FEB 16 2006.
- [13] M. S. Anwar, F. Czeschka, M. Hesselberth, M. Porcu, and J. Aarts. Long-range supercurrents through half-metallic ferromagnetic CrO₂. *PHYSICAL REVIEW B*, 82(10), SEP 3 2010.
- [14] A. Singh, S. Voltan, K. Lahabi, and J. Aarts. Colossal proximity effect in a superconducting triplet spin valve based on the half-metallic ferromagnet cro₂. *Phys. Rev. X*, 5:021019, May 2015.
- [15] X. L. Wang, A. Di Bernardo, N. Banerjee, A. Wells, F. S. Bergeret, M. G. Blamire, and J. W. A. Robinson. Giant triplet proximity effect in superconducting pseudo spin valves with engineered anisotropy. *PHYSICAL REVIEW B*, 89(14), APR 30 2014.
- [16] M. S. Anwar, M. Veldhorst, A. Brinkman, and J. Aarts. Long range supercurrents in ferromagnetic CrO₂ using a multilayer contact structure. *Appl. Phys. Lett.*, 100(5), JAN 30 2012.
- [17] A. Gupta, X. W. Li, S. Guha, and Gang Xiao. Selective-area and lateral overgrowth of chromium dioxide (cro₂) films by chemical vapor deposition. *Applied Physics Letters*, 75(19), 1999.
- [18] Xiaojing Zou and Gang Xiao. Magnetic domain configurations of epitaxial chromium dioxide (cro₂) nanostructures. *Applied Physics Letters*, 91(11), 2007.
- [19] Isaac H. Wildeson, David A. Ewoldt, Robert Colby, Eric A. Stach, and Timothy D. Sands. Controlled growth of ordered nanopore arrays in gan. *Nano Letters*, 11(2):535–540, 2011. PMID: 21171632.
- [20] Y. D. Wang, K. Y. Zang, S. J. Chua, S. Tripathy, P. Chen, and C. G. Fonstad. Nanoair-bridged lateral overgrowth of gan on ordered nanoporous gan template. *Applied Physics Letters*, 87(25), 2005.
- [21] Zheleva T. S., Smith A. S., Thomson D. B., Linthicum K. J., Rajagopal P., and Davis R. F. . Pendeo-epitaxy: A new approach for lateral growth of gallium nitride films. *Journal of Electronic Materials*, 28(4), 1999.
- [22] A. et al. Tanaka. Strong geometrical effects in submillimeter selective area growth and light extraction of gan light emitting diodes on sapphire. *Sci. Rep.*, 5(19), 1999.
- [23] Thomas E. Vandervelde, Piyush Kumar, Takeshi Kobayashi, Jennifer L. Gray, Tim Pernel, Jerrold A. Floro, Robert Hull, and John C. Bean. Growth of quantum fortress structures in silxgex/si via combinatorial deposition. *Applied Physics Letters*, 83(25):5205–5207, 2003.
- [24] Xue Wang, Jana Hartmann, Martin Mandl, Matin Sadat Mohajerani, Hergo-H. Wehmann, Martin Strassburg, and Andreas Waag. Growth kinetics and mass transport mechanisms of gan columns by selective area metal organic vapor phase epitaxy. *Journal of Applied Physics*, 115(16), 2014.
- [25] C. König, M. Fonin, M. Laufenberg, A. Biehler, W. Bühner, M. Kläui, U. Rüdiger, and G. Güntherodt. Micromagnetism and magnetotransport properties of micron-sized epitaxial cro₂ (100) wires. 75:144428, Apr 2007.
- [26] A. Biehler, M. Kläui, M. Fonin, C. König, G. Güntherodt, and U. Rüdiger. Micromagnetism and magnetotransport properties of micron-sized epitaxial cro₂ (100) wires. 75:184427, Apr 2007.
- [27] S. P. Lewis, P. B. Allan, and T. Sasaki. Band structure and transport properties of cro₂. 55:10253, 1997.